Realizing One-Dimensional Electronic States in Graphene via Coupled Zeroth Pseudo-Landau Levels

Yi-Wen Liu,[1,‡] Zhen Zhan,[2,‡] Zewen Wu,[2] Chao Yan,[1] Shengjun Yuan,[2,3,*] and Lin He[1,†]
[1]Center for Advanced Quantum Studies, Department of Physics, Beijing Normal University, Beijing, 100875, People's Republic of China
[2]Key Laboratory of Artificial Micro- and Nano-structures of the Ministry of Education and School of Physics and Technology, Wuhan University, Wuhan 430072, China
[3]Wuhan Institute of Quantum Technology, Wuhan 340206, China

(Received 10 November 2021; revised 17 June 2022; accepted 6 July 2022; published 28 July 2022)

Strain-induced pseudomagnetic fields can mimic real magnetic fields to generate a zero-magnetic-field analog of the Landau levels (LLs), i.e., the pseudo-Landau levels (PLLs), in graphene. The distinct nature of the PLLs enables one to realize novel electronic states beyond what is feasible with real LLs. Here, we show that it is possible to realize exotic electronic states through the coupling of zeroth PLLs in strained graphene. In our experiment, nanoscale strained structures embedded with PLLs are generated along a one-dimensional (1D) channel of suspended graphene monolayer. Our results demonstrate that the zeroth PLLs of the strained structures are coupled together, exhibiting a serpentine pattern that snakes back and forth along the 1D suspended graphene monolayer. These results are verified theoretically by large-scale tight-binding calculations of the strained samples. Our result provides a new approach to realizing novel quantum states and to engineering the electronic properties of graphene by using localized PLLs as building blocks.

DOI: 10.1103/PhysRevLett.129.056803

A nonuniform strain in graphene can create pseudomagnetic fields (PMFs), which generate a distinct Landau quantization at zero external magnetic fields [1–6]. By tuning the deformed structure of graphene, the PMFs can be changed from zero to hundreds of tesla, providing an efficient way to tailor the electronic properties of graphene at the nanoscale [7–24]. Therefore, many efforts have been made to introduce custom-designed strained structures [25–28] and create PMFs in graphene [16–20]. Even more interestingly, the different nature between the PMFs and the real magnetic fields enables one to realize novel quantum states that cannot be realized purely with the real magnetic fields [15–20]. For example, a special valley-polarized Landau quantization was observed in strained graphene because the PMFs point in opposite directions at the two different valleys of graphene and a combination of the PMFs and real magnetic fields leads to imbalanced effective magnetic fields at distinct valleys [14,21]. The opposite directions of the PMFs in the two valleys result in sublattice polarization of the zeroth pseudo-Landau levels (PLLs) that is not present for real LLs [13,19]. Moreover, the PLLs are generated by the deformed structure of graphene and can be localized at the nanoscale. In this Letter, by taking advantage of the nanoscale localization of PLLs, we demonstrate the realization of novel quantum states by using the PLLs as building blocks. We realize one-dimensional (1D) electronic states in graphene via coupled zeroth PLLs, which are directly visualized in our scanning tunneling microscopy (STM) measurements and supported by a full tight-binding calculation.

In our experiment, strained structures are generated along 1D channels of the suspended graphene monolayer. To obtain the 1D channels, we adopt an etching technique using high flow of hydrogen and metallic nanoparticles [29–35]. The width of etched 1D channels ranges from a few nanometers to several tens of nanometers (see Supplemental Material, Figs. S1 and S2 [36]). Two types of 1D channels are obtained after etching processes, as summarized in Fig. 1. The first one is that both the topmost graphene and the underlying graphene layers are etched and the 1D trench with atomic-scale sharp edges of the topmost graphene is shown in Figs. 1(a) and 1(c). The second one is that the underlying graphene layers are etched, leaving the topmost graphene layer untouched, as shown in Figs. 1(b) and 1(e). These two types of the 1D channels are quite different in the heights of trenches and the strengths of the intervalley scattering around them, as shown in Figs. 1(d) and 1(f). The $(\sqrt{3}\times\sqrt{3})R30°$ pattern only can be observed in the first case because rough edges at the atomic scale result in strong intervalley scattering in graphene. In this work, we mainly focused on the bottom-etched channel because that it provides 1D nanoscale suspended graphene monolayer.

For most of the 1D suspended graphene membrane (the 1D structure above large Ni terraces or multilayer graphene terraces), the length is over several hundreds of nanometers

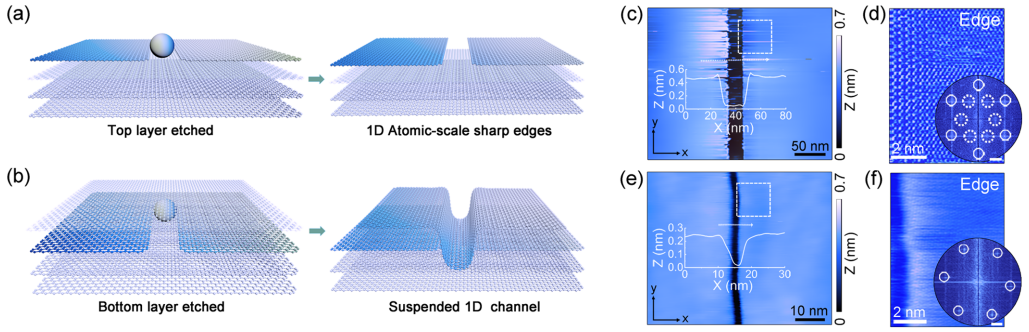

FIG. 1. (a) and (b) Depiction of the top (bottom) layer etched edges. (c) A STM image of top etched sharp edges, $V_s = 1.4$ V, $I = 0.6$ nA. Inset: height profile across the edge. (d) Close-up atomic and FFT image of the square area in (c), $V_s = 0.4$ V, $I = 0.5$ pA. Outer spots are the reciprocal lattices of graphene. The inner pattern is induced by intervalley scattering. Scale bar: 3.5 nm^{-1}. (e) A STM image of the bottom etched smooth channel, $V_s = -0.8$ V, $I = 0.2$ pA. (f) Close-up atomic and FFT image of the square area in (e). $V_s = 0.6$ V, $I = 0.1$ nA. Scale bar: 3.5 nm^{-1}.

and there is no observable strained structure (Supplemental Material, Figs. S1 and S2 [36]). However, for the 1D suspended graphene monolayer above terraces with small widths, we observe clearly strained structures along the 1D structure, as shown in Figs. 2(a)–2(c) (see Supplemental Material, Figs. S3 to S4 for more characterizations [36]). In this case, the 1D suspended graphene monolayer is suddenly cut off at the edges of the small terraces, which may introduce strain in the short 1D suspended graphene monolayer and, consequently, generate approximately periodic ripples along it, as shown in Fig. 2(b) (see Supplemental Material, Fig. S5 for other samples [36]). The lattice constants are measured on the ripples and the C—C bonds exhibit a variation of about 2% along two orientations, suggesting that a tensile strain is generated on the crest of ripples (see Supplemental Material, Fig. S6 for the detailed analysis [36]) [42,43].

In strained graphene, lattice deformation can effectively modulate electron hopping and create PLLs around the Dirac point of graphene. The strain-induced PLLs can be explicitly demonstrated by scanning tunneling spectroscopy (STS) measurements [7–14,16–23]. Figure 2(d)

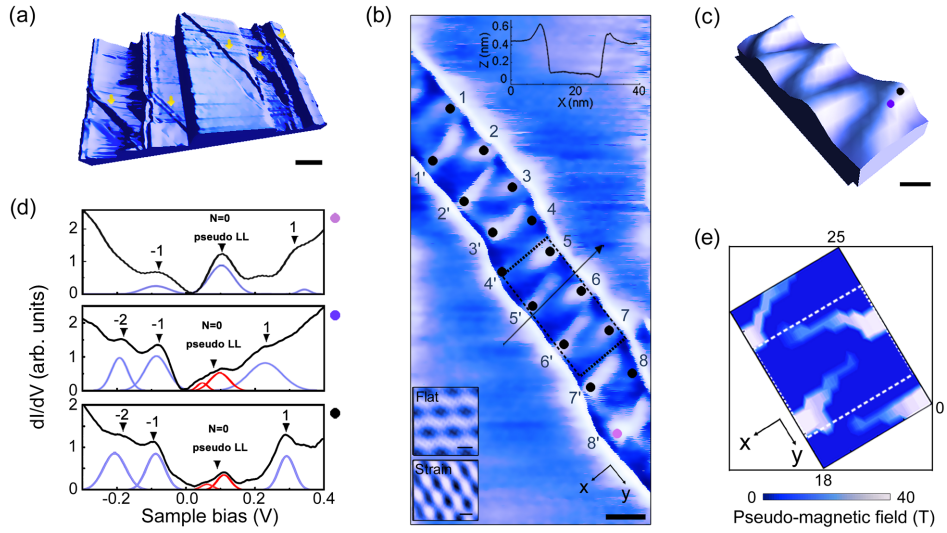

FIG. 2. (a) A STM image of 1D channels on steps, $V_s = -1.8$ V, $I = 0.1$ nA. Scale bar: 20 nm. (b) Two-dimensional projection of the longest channel in (a). The heads of ripples are labeled with black dots and numbers. Note that the ripples labeled as 4 and 8 are difficult to be observed due to the small height. $V_s = 0.05$ V, $I = 0.015$ nA. Scale bar: 10 nm. Inset: the height profile along the black arrow. The square frames of the insets show the triangular (hexagonal) lattice image on (off) the ripple. $V_s = 0.1$ V, $I = 0.04$ nA. Scale bar: 0.2 nm. (c) Close-up image of the black frame in (b). Scale bar: 3 nm. (d) Top panel is the dI/dV spectrum taken at the pink dot in (b). The PMF is about 29 T, and the full width at half maximum (FWHM) of the zeroth PLL is 75 meV. Middle panel is the dI/dV spectrum taken at the purple dot in (c). The splitting and FWHM of the zeroth PLLs are 56 and 110 meV, respectively. Bottom panel is the dI/dV spectrum taken at the black dot in (c). The splitting and FWHM of the zeroth PLLs are 62 and 112 meV, respectively. The purple and red solid lines are the fittings of the PLLs. (e) The distribution of PMFs in region I, which is extracted from experimental STS curves.

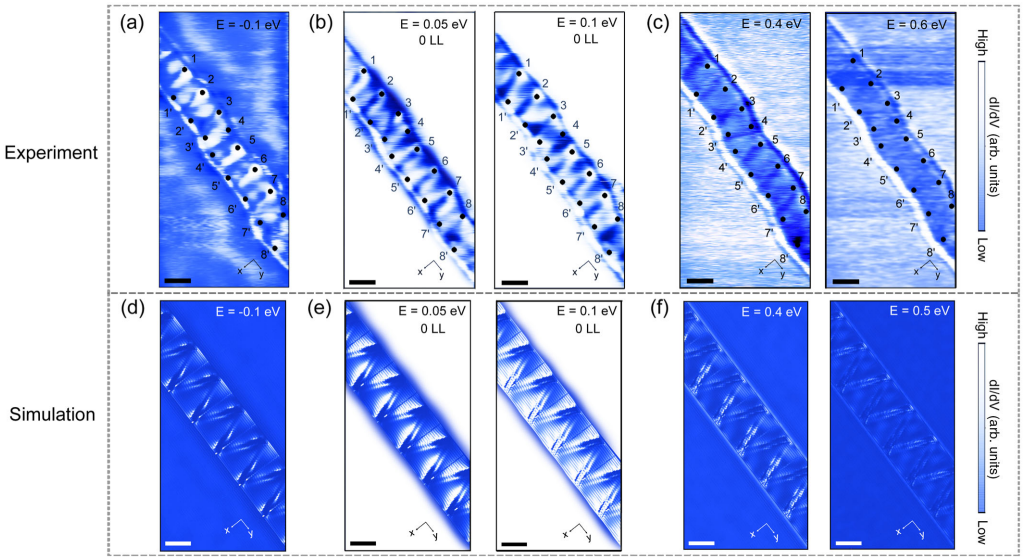

FIG. 3. dI/dV maps measured at the energy of (a) −0.1 eV, (b) 0.05 eV and 0.1 eV (around the zeroth PLL), (c) 0.4 eV and 0.6 eV. (d)–(f) Theoretical calculated LDOS maps at the corresponding energies of −0.1 eV, 0.05 eV, 0.1 eV, 0.4 eV, and 0.5 eV. Scale bar: 10 nm. All images in the experiment or simulation have the same color scale.

shows representative STS spectra measured on different positions of the strained structure [marked in Fig. 2(c)] at 77 K. The pronounced peaks are attributed to the strain-induced PLLs, which can be fitted well by the Landau quantization of massless Dirac fermions in graphene monolayer (see Supplemental Material, Fig. S7 for fitting of the PLLs [36]). In our experiment, a robust zeroth PLL is observed in spectra measured on positions with large strain in the 1D channel. In contrast to the hexagonal lattice off the ripple, the triangular lattice, as shown in the inset of Fig. 2(b), is observed in the strained region at the energy of the zeroth PLLs. The observed triangular lattice can further confirm the nature of the zeroth PLLs in strained graphene [13,19]. To measure the spatial distribution of the PMFs, STS spectra at different positions of the 1D suspended graphene monolayer are carefully measured. The values of the PMFs in each position of the strained structures can be obtained according to the fitting of the Landau quantization. Figure 2(e) shows the distribution of the PMFs measured around four strained ripples along the 1D suspended graphene monolayer. The PMFs are quite nonuniform and show a maximum value on one side of the ripple (ripple head) and a minimum value on the other side (ripple tail). Notably, the PMFs exhibit a similar period as the strained structures along the 1D structure.

In our experiment, the zeroth PLLs in the strained ripples are quite different [Fig. 2(d)]. For a small partial of the ripples, such as the ripple labeled as 8′, there is only one peak with a bandwidth of about 75 meV for the zeroth PLL. However, for most of the ripples, such as the ripple labeled as 7, the bandwidth of the zeroth PLL is as large as 110 meV and the zeroth PLL seems to be consisting of two peaks (see Supplemental Material, Figs. S7 and S8 for more data [36]). Such a difference is attributed to the different coupling of the zeroth PLL between adjacent ripples. For the ripple 8′, the distance between adjacent ripples is relatively large and, therefore, the coupling of the zeroth PLL between adjacent ripples is quite weak. For the ripple 7, the small distance between adjacent ripples enables strong coupling of the zeroth PLL and, consequently, broadens the zeroth PLL. Here, we should point out that the spatial extent of the zeroth PLL goes as $l_B = \sqrt{(\hbar/eB)}$ ($\hbar$ is the reduced Plank constant, e is the electric charge, and B is the PMFs), therefore, a decrease of the PMF will enhance coupling between the zeroth PLL and result in a larger bandwidth of the zeroth PLL.

The coupling of the zeroth PLL is further confirmed by carrying out measurements of conductance maps, which reflect the spatial-distributed local density of states (LDOS), at different energies, as shown in Figs. 3(a)–3(c) (see Supplemental Material, Fig. S9 for more maps [36]). At both positive and negative energies, far away from the zeroth PLL, there is almost no serpentine feature induced by the strained structures [Fig. 3(c)]. By reducing the energy to approach the zeroth PLL, strain-induced electronic states are observed along the 1D structure [Fig. 3(a)]. At the zeroth PLL energy, shown in Fig. 3(b), we observe a serpentine pattern that snakes back and forth along the 1D suspended graphene monolayer, arising from the coupling of the zeroth PLL between adjacent ripples. In contrast to higher PLLs, the states of the zeroth PLL are more robust because they are independent of the PMF strength.

The serpentine pattern is further verified by utilizing a large-scale propagation method in the framework of tight-binding model. The strained graphene used in the calculation is composed of transverse (x) buckling and

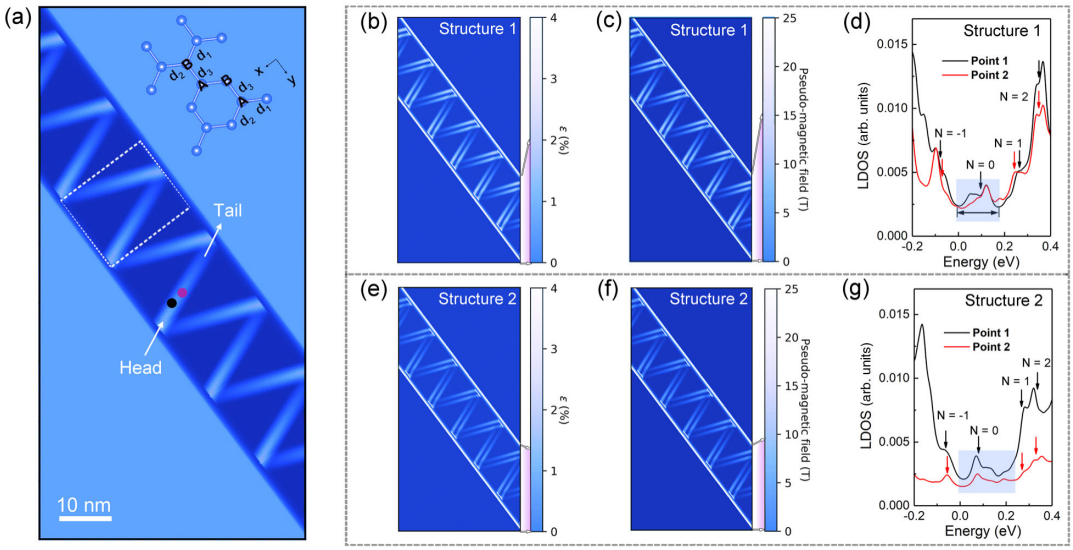

FIG. 4. (a) Schematic representation of the calculated graphene monolayer embedded with buckling and periodic ripples that have crests at an angle to the trench. The unit cell is marked with a white dotted frame. Inset: the armchair configuration along the channel. (b) and (e) Contour plots of the calculated average strain ε of strained graphene structures 1 and 2, respectively. The pink areas denote the ranges of the strain. (c) and (f) Calculated PMFs of structures 1 and 2. (d) and (g) Calculated LDOS of points 1 and 2 along ripples of structures 1 and 2, respectively. The corresponding positions are marked by black and red dots in (a). LLs indices are marked in figures.

longitudinal (y) ripples (see Supplemental Material, Fig. S10 for details [36]). The out-of-plane displacements of buckling ζ_b and of ripples ζ_r are described as

$$\zeta_b = \begin{cases} -h, & |x| < \frac{W}{4}, \\ -h^*\left(\frac{4^*|x|}{W} - 1\right)^{pow}, & \frac{W}{4} \le |x| \le \frac{W}{2}, \end{cases} \tag{1}$$

$$\zeta_r = A\sin(2\pi y/\lambda), \tag{2}$$

where h and A are the amplitudes, W is the width of the trench, and λ is the wavelength. The parameter pow describes the shape of the buckling. Five setting parameters h, A, W, λ, and pow of buckling and ripples are modulated to mimic the strained structure inside the black dashed rectangle in Fig. 2(b), and obtain the structure 1 in Fig. 4(a). The distortion-induced strain is defined as $\varepsilon = [(\sum_i d_i/3d) - 1] \times 100\%$ with d_i ($i = 1,2,3$) the first neighbor interatomic distance in the deformed lattice and $d = 0.142$ nm. As illustrated in Fig. 4(b), the ε shows a periodicity and with the maximum value around 4% located around the crossover (ripple head) of the buckling and ripples. The strength of the strain-induced PMFs in the 1D suspended graphene monolayer is evaluated in Fig. 4(c). The PMFs exhibit the same period as the strained structure, which is in good agreement with the experimental results.

Figure 4(d) shows representative LDOS at two different positions of the strained structure. The strain-induced PLLs can be explicitly identified. To further compare with the experimental result, we calculate energy-fixed LDOS of the 1D suspended graphene monolayer, as shown in Figs. 3(d)–3(f). Similar to the experimental results, the 1D winding states, exhibiting a serpentine pattern, are only observed at the zeroth PLL energy (see Supplemental Material, Fig. S11 for more cases [36]). The ripples in Fig. 4(a) have varied amplitude A along the ripples, and the strain decreases from the ripple head to tail. This feature excludes the possibility of connecting highly localized states induced by the strain in the ripples to form a snake-like pattern (see Supplemental Material, Fig. S12 for details of discussion [36]). More importantly, the generation of coupled ripples does not require atomically precise control of strain (see Supplemental Material, Figs. S13 and S14 [36]), which provides a new approach to exploring the interactions of localized states at a large spatial scale [44,45].

To further explore the effects of strain, we carry out more calculations of reducing the strain near the ripple head by decreasing 25% of the amplitude A (see Supplemental Material, Fig. S15 [36]), as shown in Fig. 4(e) of structure 2. The PMF of this structure, as shown in Fig. 4(f), shows lower intensity and the width of zero-mode increases from 180 to 250 meV. With the decrease of the PMFs, the pseudomagnetic length increases, and the spatial extension of the wavefunction becomes wider. Consequently, the tunneling between two ripples increases and results in a larger bandwidth. Moreover, we find that for the coupled PLLs, the noteworthy spitting of PLLs is presented, which is consistent with the experimental results (see Supplemental Material, Fig. S16 for the theoretical result about the sublattice polarized zeroth LLs [36]). Last but not least, a Su-Schrieffer-Heeger (SSH) metallic state could be realized if periodic ripples are generated along the 1D channel (Supplemental Material, Fig. S17 [36]) [44–47].

In summary, we demonstrate the realization of the 1D snakelike states in graphene by using the strain-induced PLLs as building blocks. Via STM and STS measurements, we directly image the realized electronic states. Our result provides a new avenue to build custom-designed model systems, such as the SSH chain [46,47], Lieb lattice, and kagome lattice [48–51], via coupled PLLs.

This work was supported by the National Key R and D Program of China (Grants No. 2021YFA1401900, No. 2021YFA1400100, No. 2017YFA0303301, and No. 2018YFA0305800) and National Natural Science Foundation of China (Grants No. 12141401, No. 11974050, No. 11921005, No. 11774269, No. 12047543). Numerical calculations presented in this Letter were performed on the supercomputing system in the Supercomputing Center of Wuhan University.

*To whom all correspondence should be addressed.
s.yuan@whu.edu.cn
†To whom all correspondence should be addressed.
helin@bnu.edu.cn
‡These authors contributed equally to this work.

[1] M. A. Vozmediano, M. Katsnelson, and F. Guinea, Gauge fields in graphene, Phys. Rep. **496**, 109 (2010).
[2] F. Guinea, B. Horovitz, and P. Le Doussal, Gauge field induced by ripples in graphene, Phys. Rev. B **77**, 205421 (2008).
[3] F. Guinea, M. Katsnelson, and M. Vozmediano, Midgap states and charge inhomogeneities in corrugated graphene, Phys. Rev. B **77**, 075422 (2008).
[4] F. Guinea, M. Katsnelson, and A. Geim, Energy gaps and a zero-field quantum Hall effect in graphene by strain engineering, Nat. Phys. **6**, 30 (2010).
[5] S. Zhu, J. A. Stroscio, and T. Li, Programmable Extreme Pseudomagnetic Fields in Graphene by a Uniaxial stretch, Phys. Rev. Lett. **115**, 245501 (2015).
[6] B. Amorim, A. Cortijo, F. De Juan, A. G. Grushin, F. Guinea, A. Gutiérrez-Rubio, H. Ochoa, V. Parente, R. Roldán, and P. San-Jose, Novel effects of strains in graphene and other two dimensional materials, Phys. Rep. **617**, 1 (2016).
[7] N. Levy, S. Burke, K. Meaker, M. Panlasigui, A. Zettl, F. Guinea, A. C. Neto, and M. F. Crommie, Strain-induced pseudo–magnetic fields greater than 300 tesla in graphene nanobubbles, Science **329**, 544 (2010).
[8] D. Guo, T. Kondo, T. Machida, K. Iwatake, S. Okada, and J. Nakamura, Observation of Landau levels in potassium-intercalated graphite under a zero magnetic field, Nat. Commun. **3**, 1068 (2012).
[9] J. Lu, A. H. Castro Neto, and K. P. Loh, Transforming moiré blisters into geometric graphene nano-bubbles, Nat. Commun. **3**, 823 (2012).
[10] H. Yan, Y. Sun, L. He, J.-C. Nie, and M. H. Chan, Observation of Landau-level-like quantization at 77 K along a strained-induced graphene ridge, Phys. Rev. B **85**, 035422 (2012).
[11] W. Yan, W.-Y. He, Z.-D. Chu, M. Liu, L. Meng, R.-F. Dou, Y. Zhang, Z. Liu, J.-C. Nie, and L. He, Strain and curvature induced evolution of electronic band structures in twisted graphene bilayer, Nat. Commun. **4**, 2159 (2013).
[12] L. Meng, W.-Y. He, H. Zheng, M. Liu, H. Yan, W. Yan, Z.-D. Chu, K. Bai, R.-F. Dou, and Y. Zhang, Strain-induced one-dimensional Landau level quantization in corrugated graphene, Phys. Rev. B **87**, 205405 (2013).
[13] A. Georgi, P. Nemes-Incze, R. Carrillo-Bastos, D. Faria, S. Viola Kusminskiy, D. Zhai, M. Schneider, D. Subramaniam, T. Mashoff, and N. M. Freitag, Tuning the pseudospin polarization of graphene by a pseudomagnetic field, Nano Lett. **17**, 2240 (2017).
[14] S.-Y. Li, Y. Su, Y.-N. Ren, and L. He, Valley Polarization and Inversion in Strained Graphene via Pseudo-Landau Levels, Valley Splitting of Real Landau Levels, and Confined States, Phys. Rev. Lett. **124**, 106802 (2020).
[15] P. Nigge, A. Qu, É. Lantagne-Hurtubise, E. Mårsell, S. Link, G. Tom, M. Zonno, M. Michiardi, M. Schneider, and S. Zhdanovich, Room temperature strain-induced Landau levels in graphene on a wafer-scale platform, Sci. Adv. **5**, eaaw5593 (2019).
[16] R. Banerjee, V.-H. Nguyen, T. Granzier-Nakajima, L. Pabbi, A. Lherbier, A. R. Binion, J.-C. Charlier, M. Terrones, and E. W. J. N. l. Hudson, Strain modulated superlattices in graphene, Nano Lett. **20**, 3113 (2020).
[17] X. Zong, H. Hu, G. Ouyang, J. Wang, R. Shi, L. Zhang, Q. Zeng, C. Zhu, S. Chen, and C. Cheng, Tailoring sample-wide pseudo-magnetic fields on a graphene–black phosphorus heterostructure, Nat. Nanotechnol. **13**, 828 (2018).
[18] P. Jia, W. Chen, J. Qiao, M. Zhang, X. Zheng, Z. Xue, R. Liang, C. Tian, L. He, Z. Di, and X. Wang, Programmable graphene nanobubbles with three-fold symmetric pseudo-magnetic fields, Nat. Commun. **10**, 3127 (2019).
[19] J. Mao, S. P. Milovanović, M. Anđelković, X. Lai, Y. Cao, K. Watanabe, T. Taniguchi, L. Covaci, F. M. Peeters, and A. K. Geim, Evidence of flat bands and correlated states in buckled graphene superlattices, Nature (London) **584**, 215 (2020).
[20] Y. Jiang, J. Mao, J. Duan, X. Lai, K. Watanabe, T. Taniguchi, and E. Y. Andrei, Visualizing strain-induced pseudomagnetic fields in graphene through an hBN magnifying glass, Nano Lett. **17**, 2839 (2017).
[21] S.-Y. Li, K.-K. Bai, L.-J. Yin, J.-B. Qiao, W.-X. Wang, and L. He, Observation of unconventional splitting of Landau levels in strained graphene, Phys. Rev. B **92**, 245302 (2015).
[22] C.-C. Hsu, M. Teague, J.-Q. Wang, and N.-C. Yeh, Nano-scale strain engineering of giant pseudo-magnetic fields, valley polarization, and topological channels in graphene, Sci. Adv. **6**, eaat9488 (2020).
[23] H. Shi, Z. Zhang, Z. Qi, K. Huang, E. van Veen, J. A. Silva-Guillen, R. Zhang, P. Li, K. Xie, H. Ji, M. I. Katsnelson, S. Yuan, S. Qin, and Z. Zhang, Large-area, periodic, and tunable intrinsic pseudo-magnetic fields in low-angle twisted bilayer graphene, Nat. Commun. **11**, 371 (2020).
[24] D.-H. Kang, H. Sun, M. Luo, K. Lu, M. Chen, Y. Kim, Y. Jung, X. Gao, S. J. Parluhutan, J. Ge, S. W. Koh, D. Giovanni, T. C. Sum, Q. J. Wang, H. Li, and D. Nam, Pseudo-magnetic field-induced slow carrier dynamics in

periodically strained graphene, Nat. Commun. **12**, 5087 (2021).
[25] W. Bao, F. Miao, Z. Chen, H. Zhang, W. Jang, C. Dames, and C. N. Lau, Controlled ripple texturing of suspended graphene and ultrathin graphite membranes, Nat. Nanotechnol. **4**, 562 (2009).
[26] L. Tapasztó, T. Dumitrică, S. J. Kim, P. Nemes-Incze, C. Hwang, and L. P. J. N. p. Biró, Breakdown of continuum mechanics for nanometre-wavelength rippling of graphene, Nat. Phys. **8**, 739 (2012).
[27] L. Meng, Y. Su, D. Geng, G. Yu, Y. Liu, R.-F. Dou, J.-C. Nie, and L. He, Hierarchy of graphene wrinkles induced by thermal strain engineering, Appl. Phys. Lett. **103**, 251610 (2013).
[28] K.-K. Bai, Y. Zhou, H. Zheng, L. Meng, H. Peng, Z. Liu, J.-C. Nie, and L. He, Creating One-Dimensional Nanoscale Periodic Ripples in a Continuous Mosaic Graphene Monolayer, Phys. Rev. Lett. **113**, 086102 (2014).
[29] L. Ci, Z. Xu, L. Wang, W. Gao, F. Ding, K. F. Kelly, B. I. Yakobson, and P. M. Ajayan, Controlled nanocutting of graphene, Nano Res. **1**, 116 (2008).
[30] L. C. Campos, V. R. Manfrinato, J. D. Sanchez-Yamagishi, J. Kong, and P. Jarillo-Herrero, Anisotropic etching and nanoribbon formation in single-layer graphene, Nano Lett. **9**, 2600 (2009).
[31] N. Severin, S. Kirstein, I. Sokolov, and J. Rabe, Rapid trench channeling of graphenes with catalytic silver nanoparticles, Nano Lett. **9**, 457 (2009).
[32] M. Lukas, V. Meded, A. Vijayaraghavan, L. Song, P. M. Ajayan, K. Fink, W. Wenzel, and R. Krupke, Catalytic subsurface etching of nanoscale channels in graphite, Nat. Commun. **4**, 1379 (2013).
[33] L. Chen, L. He, H. S. Wang, H. Wang, S. Tang, C. Cong, H. Xie, L. Li, H. Xia, T. Li, T. Wu, D. Zhang, L. Deng, T. Yu, X. Xie, and M. Jiang, Oriented graphene nanoribbons embedded in hexagonal boron nitride trenches, Nat. Commun. **8**, 14703 (2017).
[34] H. S. Wang, L. Chen, K. Elibol, L. He, H. Wang, C. Chen, C. Jiang, C. Li, T. Wu, C. X. Cong, T. J. Pennycook, G. Argentero, D. Zhang, K. Watanabe, T. Taniguchi, W. Wei, Q. Yuan, J. C. Meyer, and X. Xie, Towards chirality control of graphene nanoribbons embedded in hexagonal boron nitride, Nat. Mater. **20**, 202 (2021).
[35] R. Yang, L. Zhang, Y. Wang, Z. Shi, D. Shi, H. Gao, E. Wang, and G. Zhang, An anisotropic etching effect in the graphene basal plane, Adv. Mater. **22**, 4014 (2010).
[36] See Supplemental Material at http://link.aps.org/supplemental/10.1103/PhysRevLett.129.056803 for sample preparation, more experimental data, details of calculation, and discussion, which includes Refs. [37–41].
[37] Y.-W. Liu, C.-Y. Hao, and L. He, Tailoring the Energy Landscape of Graphene Nanostructures on Graphene and Manipulating Them Using Tilt Grain Boundaries, Phys. Rev. Applied **17**, 034013 (2022).
[38] W. Yan, S.-Y. Li, L.-J. Yin, J.-B. Qiao, J.-C. Nie, and L. He, Spatially resolving unconventional interface Landau quantization in a graphene monolayer-bilayer planar junction, Phys. Rev. B **93**, 195408 (2016).
[39] S. Yuan, H. De Raedt, and M. I. Katsnelson, Modeling electronic structure and transport properties of graphene with resonant scattering centers, Phys. Rev. B **82**, 115448 (2010).
[40] R. Haydock, V. Heine, and M. Kelly, Electronic structure based on the local atomic environment for tight-binding bands, J. Phys. C **5**, 2845 (1972).
[41] S.-C. Ho, C.-H. Chang, Y.-C. Hsieh, S.-T. Lo, B. Huang, T.-H.-Y. Vu, C. Ortix, and T.-M. Chen, Hall effects in artificially corrugated bilayer graphene without breaking time-reversal symmetry, National electronics review **4**, 116 (2021).
[42] F. F. Settembrini, F. Colangelo, A. Pitanti, V. Miseikis, C. Coletti, G. Menichetti, R. Colle, G. Grosso, A. Tredicucci, and S. Roddaro, Anisotropic straining of graphene using micropatterned SiN membranes, APL Mater. **4**, 116107 (2016).
[43] A. Rosenauer, U. Fischer, D. Gerthsen, and A. Förster, Composition evaluation of $In_xGa_{1-x}As$ Stranski-Krastanow-island structures by strain state analysis, Appl. Phys. Lett. **71**, 3868 (1997).
[44] D. J. Rizzo, G. Veber, J. Jiang, R. McCurdy, T. Cao, C. Bronner, T. Chen, S. G. Louie, F. R. Fischer, and M. F. Crommie, Inducing metallicity in graphene nanoribbons via zero-mode superlattices, Science **369**, 1597 (2020).
[45] D. J. Rizzo, G. Veber, T. Cao, C. Bronner, T. Chen, F. Zhao, H. Rodriguez, S. G. Louie, M. F. Crommie, and F. R. Fischer, Topological band engineering of graphene nanoribbons, Nature (London) **560**, 204 (2018).
[46] W. P. Su, J. R. Schrieffer, and A. J. Heeger, Solitons in Polyacetylene, Phys. Rev. Lett. **42**, 1698 (1979).
[47] W. P. Su, J. R. Schrieffer, and A. J. Heeger, Soliton excitations in polyacetylene, Phys. Rev. B **22**, 2099 (1980).
[48] R. Drost, T. Ojanen, A. Harju, and P. Liljeroth, Topological states in engineered atomic lattices, Nat. Phys. **13**, 668 (2017).
[49] M. R. Slot, T. S. Gardenier, P. H. Jacobse, G. C. van Miert, S. N. Kempkes, S. J. Zevenhuizen, C. M. Smith, D. Vanmaekelbergh, and I. Swart, Experimental realization and characterization of an electronic Lieb lattice, Nat. Phys. **13**, 672 (2017).
[50] A. Ramires and J. L. Lado, Electrically Tunable Gauge Fields in Tiny-Angle Twisted Bilayer Graphene, Phys. Rev. Lett. **121**, 146801 (2018).
[51] M. Telychko, G. Li, P. Mutombo, D. Soler-Polo, X. Peng, J. Su, S. Song, M. J. Koh, M. Edmonds, and P. Jelínek, Ultrahigh-yield on-surface synthesis and assembly of circumcoronene into a chiral electronic Kagome-honeycomb lattice, Sci. Adv. **7**, eabf0269 (2021).